

Article

An Experimental Procedure to Study the High-Speed Orthogonal Cutting of Unidirectional GFRP

Martina Panico , Luca Boccarusso * , Antonio Formisano , Giuseppe Villani and Antonio Langella 

Department of Chemical, Materials and Production Engineering DICMaPI, University of Naples Federico II, P.le Tecchio 80, 80125 Naples, Italy; martina.panico@unina.it (M.P.); aformisa@unina.it (A.F.); giuseppe.villani@unina.it (G.V.); antgella@unina.it (A.L.)

* Correspondence: luca.boccarusso@unina.it; Tel.: +39-081-7682369

Abstract: The aim of this paper is to establish a valid procedure for better understanding all of the phenomena associated with the high-speed machining of glass fiber-reinforced plastic (GFRP) composites. Both rectangular and circular specimens were machined at high cutting speeds (up to 50 m/min) in order to understand what occurred for all values of fiber orientation angles during machining operations. An innovative testing methodology was proposed and studied to investigate the phenomenon of burr formation and thus understand how to avoid it during machining operations. To this end, the forces arising during the machining process and the roughness of the resulting surface were carefully studied and correlated with the cutting angle. Additionally, the cutting surface and chip morphology formed during cutting tests were examined using a high-speed camera. Close correlations were found between the variations in the cutting forces' signals and the trends of the surface roughness and the morphology of the machined surface.

Keywords: orthogonal cutting; composite materials; cutting forces; burr; chip morphology



Citation: Panico, M.; Boccarusso, L.; Formisano, A.; Villani, G.; Langella, A. An Experimental Procedure to Study the High-Speed Orthogonal Cutting of Unidirectional GFRP. *J. Manuf. Mater. Process.* **2024**, *8*, 87. <https://doi.org/10.3390/jmmp8030087>

Academic Editor: Steven Y. Liang

Received: 27 March 2024

Revised: 16 April 2024

Accepted: 24 April 2024

Published: 26 April 2024



Copyright: © 2024 by the authors. Licensee MDPI, Basel, Switzerland. This article is an open access article distributed under the terms and conditions of the Creative Commons Attribution (CC BY) license (<https://creativecommons.org/licenses/by/4.0/>).

1. Introduction

The deployment of fiber-reinforced polymer (FRP) in various industries such as aeronautics, automotive, marine, and sports applications has become pervasive in contemporary times [1,2]. This prevalence stems from its favorable characteristics, including being lightweight, possessing fatigue and corrosion resistance, and having a high modulus, specific stiffness, and strength. Despite its flexibility to be manufactured into intricate structures with a near-net shape, machining operations, predominantly cutting, milling, and drilling, are often required to achieve dimensional precision and meet assembly requirements [3].

Although alternative machining processes exist and appear to address certain challenges, conventional methods remain favored due to cost and time efficiency considerations. Unlike metals, optimization efforts must be adapted to improve the cutting quality of FRP composites. However, the inherent inhomogeneity and anisotropy of these materials make such processes difficult, often leading to extensive damage that compromises quality and dimensional accuracy and, in severe cases, results in component failure [4].

Theoretical models and experimental applications of orthogonal cutting are essential for understanding the fundamental principles of more complex machining processes such as drilling and milling [5–7]. By analyzing cutting forces in simple models, it is possible to identify the factors influencing material removal, tool wear, and surface quality. Integrating theoretical models with experimental data enhances machining strategies, optimizing cutting conditions to increase the efficiency and quality.

According to Panico et al. [8], the machining of FRP composites presents challenges due to the heterogeneity and anisotropic properties of the material, leading to chip formation mechanisms and process force analysis dependent on the cutting angle of the fibers, as

evidenced by various experimental studies [9–13]. In addition, the abrasive nature of the fibers causes rapid and severe wear of the tools, resulting in increased cutting forces, delamination defects, burrs, and a decrease in the quality of the machined surface, as demonstrated by Maegawa et al. [14] during the milling of unidirectional (UD) carbon fiber-reinforced plastic (CFRP) materials. However, it is worth noting that the study referenced is limited to cutting conditions parallel and perpendicular to the fiber orientation, thereby excluding numerous other cutting configurations.

As known, process parameters including cutting speed, depth of cut, cutting angle, and tool geometry exert a substantial influence on the efficacy and outcome of cutting processes in composite materials [15,16]. These parameters have a very complex interaction with material properties, affecting both the quality of the machined surfaces and the overall efficiency of the machining operations. Thus, a comprehensive study necessitates the inclusion of several variables in both numerical simulations and experimental analysis. While existing research provides valuable insights into cutting composite materials, many studies do not consider the full range of relevant process parameters.

Li et al. [17] focused primarily on the fiber orientation angle and depth of cut as key factors in the chip formation mechanism. However, their study overlooks cutting angle, tool geometry, and cutting speed, which is held constant at 0.5 m/min.

Chen et al. [18] developed a force prediction model suitable for the orthogonal cutting of unidirectional CFRP composites, considering nearly all of the major variables mentioned. They employed the beams on elastic foundation theory and the minimum potential energy principle when the fiber orientation θ varied from 0° to 180° . However, it is worth noting that this study also considered cutting conditions at a low speed, specifically 1 m/min.

Investigating cutting conditions at high speeds holds significant importance from both industrial productivity and process influence perspectives. Industrial applications often require increased productivity, making high-speed cutting a priority for enhancing manufacturing efficiency. Moreover, understanding the influence of cutting speed on the process is necessary for optimizing the quality of the cut. High cutting speeds can affect various aspects of the cutting process, including heat generation, chip formation, tool wear, and the material removal mechanism. The dynamic interaction between the cutting tool and the workpiece at higher speeds introduces complexities that can significantly impact the surface finish, dimensional accuracy, and integrity of the machined components [19,20]. Therefore, thorough investigation of high-speed cutting conditions is essential for achieving productivity goals while ensuring the quality and reliability of the manufacturing process.

Although there are studies on high-speed cutting of composite materials (e.g., 400 m/min [21] and 600 m/min [22] for CFRPs), they primarily focus on milling and trimming processes. Few studies, however, address orthogonal high-speed cutting of composite materials. The following two papers serve as examples of this.

Pecat et al. [23] and An et al. [24] conducted a study on the orthogonal cutting of CFRP at high cutting speeds, up to 200 m/min. Both studies utilized rectangular specimens for their investigation, so only specific fiber orientation angles were considered. Although different cutting conditions were implemented in terms of the angle formed between the tool and fiber orientation, the use of rectangular specimens did not allow for a continuous acquisition of the characteristic forces of the process.

In addition to experimental activities, several analytical models have been developed over the years primarily to predict forces in the orthogonal cutting of UD-CFRP for specific ranges of fiber orientation [25,26]. Having an analytical model represents a valuable tool not only quantitatively but also qualitatively in an industrial context, as tool wear and hence product quality are directly correlated to the force. Furthermore, the existence of analytical models and comprehensive experimental data, which include the full range of variables affecting the process, provide the opportunity to develop numerical finite element simulation models that closely approximate the real process. This approach could substantially reduce costs and time by avoiding the need for an extensive experimental campaign covering all fiber orientation angles.

Both Calzada et al. [27] and Xu et al. [28] developed finite element simulation models for the orthogonal and oblique cutting of UD-CFRP, respectively. However, these models were constructed for a limited number of fiber orientation angles (0° , 45° , 90° , and 135° for Calzada et al., and 0° , 45° , and 90° for Xu et al.). Additionally, the issue of incomplete fiber cutting poses a challenge in acquiring the precise cutting force data crucial for analyzing the chip formation mechanism and cut quality, and understanding the influence of cutting parameters on these aspects. The primary focus of this study is to investigate the orthogonal cutting of UD laminates across the full range of fiber orientation angles using a single simple test method. To achieve this, high-speed orthogonal cutting tests were conducted on rectangular and circular specimens of UD-GFRP at a cutting speed of 25 m/min. The circular specimen design allows for continuous variation in fiber orientation relative to the cutting direction within a single test, facilitating observation of its impact on cutting force development. Additionally, two polycarbonate backing plates were bonded to the upper and lower surfaces of some samples to prevent the formation of the burrs. Subsequently, employing a cutting speed of 50 m/min, a comprehensive analysis of the high-speed orthogonal cutting of GFRP was performed across all fiber orientation angles, with and without burr defects.

The present study aims to examine chip morphology and to correlate it with cutting force trends and evaluate the machined surface quality, which is heavily influenced by material anisotropy and other cutting parameters. This approach aims to gain precise insights into the phenomenon while simultaneously optimizing all aspects of the cutting process of composite materials. At the same time, this study aims to provide a simply experimental methodology to obtain results that can also be applied to more complex machining operations for composite materials.

2. Materials and Methods

UD-GFRP laminates, measuring $410 \text{ mm} \times 410 \text{ mm} \times 3.8 \text{ mm}$, were produced by the vacuum-assisted resin transfer molding (VARTM) process, utilizing SX10 (provided by Mates [29]) epoxy resin and 20 layers of unidirectional glass fiber fabric (provided by Dalla Betta group S.r.l [30]), characterized by an areal density of 300 g/m^2 . The mechanical properties of the glass fiber fabric are shown in Table 1. The average fiber volume content of the UD-GFRP laminates was about 48% and the mechanical properties are listed in Table 2. From these laminates, two types of specimens were extracted: circular specimens, 200 mm in diameter, and rectangular specimens, $400 \text{ mm} \times 100 \text{ mm}$. For the rectangular specimens, four values of fiber orientation angle were considered, i.e., 0° , 45° , 90° , and 135° .

Table 1. Mechanical properties of unidirectional glass fiber fabric [30].

Fiber Strength [MPa]	Fiber Stiffness [GPa]	Weight [g/m^2]	Thickness [mm]	Fabric Strength [kN/m]
3100	80	300	0.115	354.96

Table 2. Mean values of mechanical properties of UD-GFRP laminate.

Modulus	[GPa]
Longitudinal Modulus, E_1	45
Transverse Modulus, E_2	7
Ultimate Strengths	[MPa]
Longitudinal Tensile Strength, X_t	1320
Longitudinal Compressive Strength, X_c	810

In addition, in order to understand the influence of the burr defect on the characteristic forces of the process, as will be explained in Section 3.1, additional samples were made. In details, for some samples, on both surfaces, two plates of polycarbonate (1 mm thick) were bonded with a 0.5 mm thick layer of Araldite 2021 structural adhesive in order to avoid the

formation of burrs. In addition, as will be explained in Section 3.1, samples made of only two bonded plates of polycarbonate were made.

Cutting tests were carried out on a five-axis CNC machine (C.B. Ferrari). Figures 1 and 2 show the test bench configurations for the two different specimen geometries. The configuration for the rectangular specimen is that the feed motion is totally assigned to the tool mounted on the spindle while the component is fixed (see Figure 1). Conversely, in the case of the circular test specimen, the tool is fixed, and the motion is attributed to the machine spindle. The composite disc is rigidly assembled to the machine spindle and both cutting motion (rotation around the vertical axis) and feeding motion (movement in the direction of the tool) are assigned to it (see Figure 2). Tools made of high-speed steel (HSS), with a cutting edge width of 10 mm, which is greater than the thickness of the discs to be machined, were used. Therefore, the conditions for the execution of free orthogonal cutting were guaranteed.

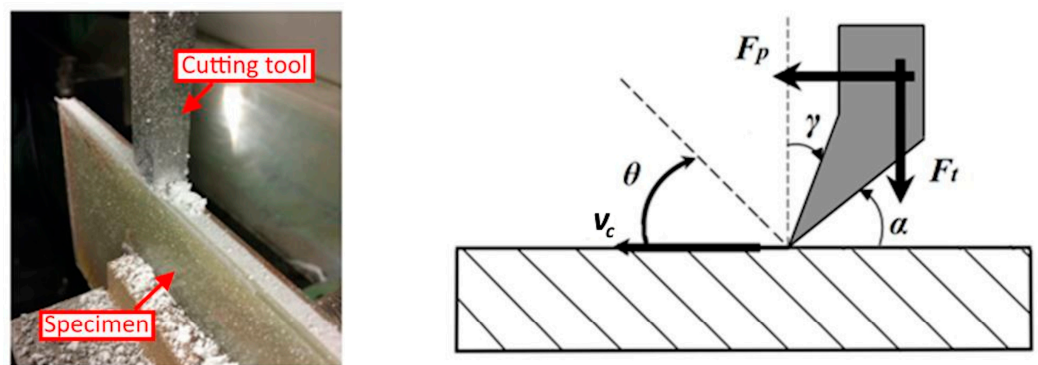


Figure 1. Rectangular specimen: cutting test (left) and its schematization (right).

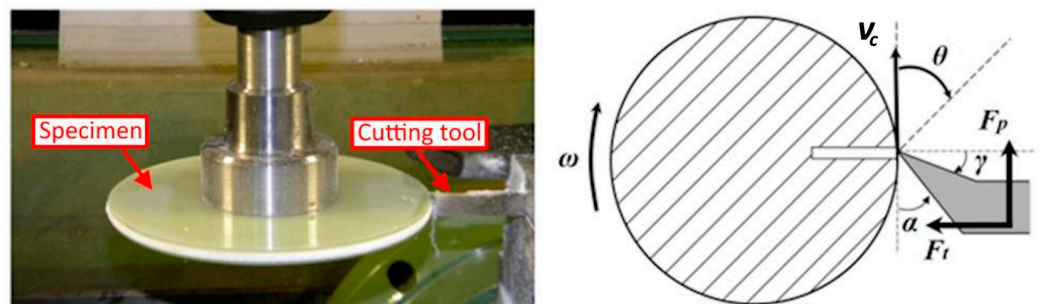


Figure 2. Circular specimen: cutting test (left) and its schematization (right).

Figures 1 and 2 show, respectively, for rectangular and circular specimens, the cutting test (left) and their schematization (right), in which features like the cutting angles (relief angle α and rake angle γ), the cutting speed (v_c), the fiber orientation angle (θ), and the principal and thrust forces (F_p and F_t) are indicated. In detail, F_p refers to the component of the cutting force that acts parallel to the cutting surface and is responsible for the deformation of the material during the cutting process, while F_t is perpendicular to the latter, as well as to the cutting surface. As shown in Figure 2, for the circular specimens, a single radial notch was created. This is necessary to detect θ during the rotation of the specimen. In fact, the notch causes a sudden decrease in the forces value, allowing for the setting up of a reference point to identify θ .

Two sets of tests were considered. The first one was carried out on both types of specimens to investigate if the circular specimens could overcome the limitation related to the rectangular ones. The phenomenon of burrs, cutting forces, and surface roughness were analyzed. A comparison was carried out for two combinations of process parameters; specifically, the tools had $\gamma = 0^\circ$ and $\alpha = 30^\circ$, $v_c = 25$ m/min, and the depth of cut, a_c , was

equal to 0.1 and 0.2 mm. To ensure a cutting speed of 25 m/min, a spindle rotation speed of 125 rpm was defined for the circular specimens.

A second set of tests, carried out on the circular specimens, was primarily considered to analyze chip morphology, with v_c equal to 50 m/min and a_c equal to 0.05, 0.1, 0.15, and 0.2 mm. The tool angles were varied: the range of γ was $0^\circ \div 30^\circ$, and the range of α was $5^\circ \div 30^\circ$. To ensure a cutting speed of 50 m/min, a spindle rotation speed of 250 rpm was defined for the circular specimens.

As the present work aims to offer a methodology applicable to the most complex machining processes (e.g., drilling and milling), the high cutting speed values of 25 m/min and 50 m/min were selected as belonging to the range of technological interest [31].

Regarding the tests on the circular specimens, five revolutions were enough for the analyses; consequently, the cutting speed can be considered constant during each test, although the rotation speed did not change. In fact, by considering the cutting condition with the greatest amount of material removed (a depth of cut equal to 0.2 mm), there was a reduction in the radius equal to 1 mm and a reduction in the cutting speed equal to 1%.

During the tests, F_p and F_t were recorded using a KISTLER 9257A load cell and the data were stored using the NI 9239 board and VBA acquisition software (Vibration Basic Analyzer VBA 1.0 B). In the test configuration with the circular specimens, the (fixed) tool was mounted on the load cell. Conversely, the configuration for the rectangular specimens required it to be rigidly mounted on the load cell. As an example, Figure 3 shows the test set-up diagram for the circular specimens.

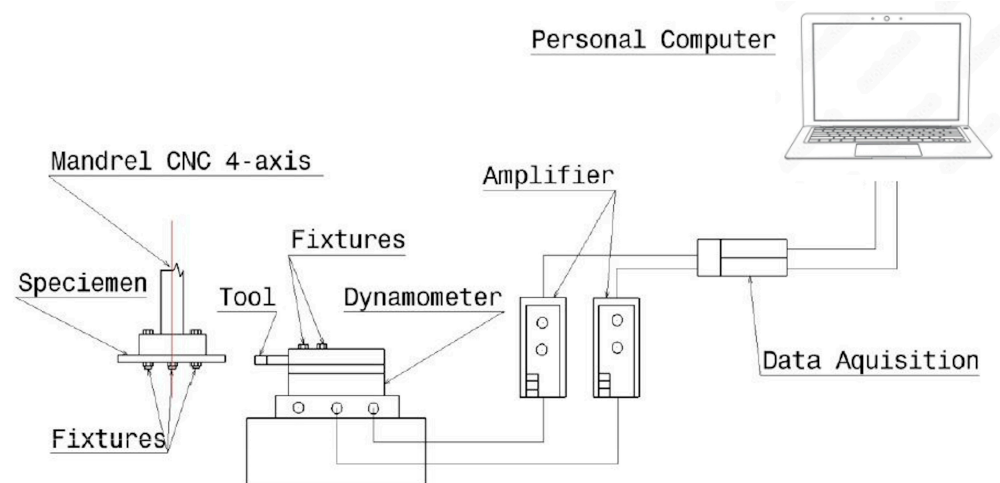


Figure 3. Example diagram of test set-up used for circular specimens.

An Olympus high-speed camera was used to acquire the images of the cutting zone for the analysis of chip morphology. The forces were recorded at a high sample rate equal to 25,000 Hz. To evaluate the quality of the machined surface, roughness measurements were carried out by using a confocal microscope (Sensofar S). Finally, a visual inspection was conducted using an optical microscope.

3. Results and Discussion

The following results are related to the first (Sections 3.1–3.3) and the second set of tests (Section 3.4).

3.1. Burrs

It is important to observe that during the orthogonal cutting of unidirectional composites, a characteristic defect appears when θ increases; this can be referred to as “burrs” [32]. The burrs (Figure 4a,b) are formed on the workpiece below the trim plane where it is possible to see some cracks; these cracks are extended for a length, d , of some millimeters

within the workpiece along the fiber direction. At the same time, two thin layers, severely bending out of plane, are created at the unsupported edges of the workpiece (Figure 4c).

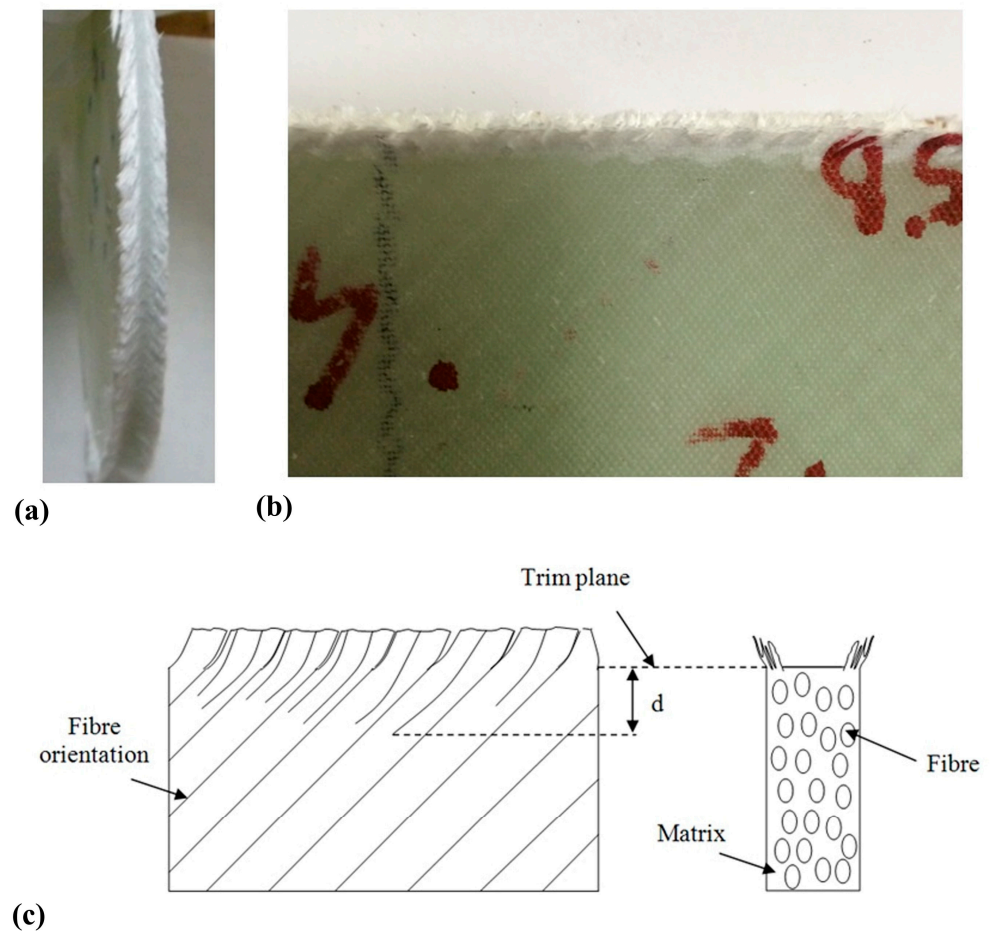


Figure 4. Burrs observed on circular (a) and rectangular (b) specimens and schematization of their formation (c).

These layers are formed by uncut fibers that pass below the tool and against the tool flank. This determines poor cut quality and causes unacceptable subsurface damage to the workpiece. Additionally, the main problem in the generation of these defects is their variability in terms of the degree of surface damage, the number of layers involved in the thickness direction, and the range of fiber orientation angles that are involved in the damage. It depends not only on the fiber volume fraction of the material being processed but also on different cutting conditions and the geometry of the tool, in particular γ [33].

In this study, to avoid the formation of burrs, two plates of polycarbonate are bonded with a structural adhesive on the upper and lower surface of the circular and rectangular specimens.

3.2. Cutting Forces

For the evaluation of the cutting forces, both depth of cut values are considered on specimens without and with polycarbonate. Three specimens are tested for each condition. Figures 5–12 in this section refer to the typical trends of F_p and F_t .

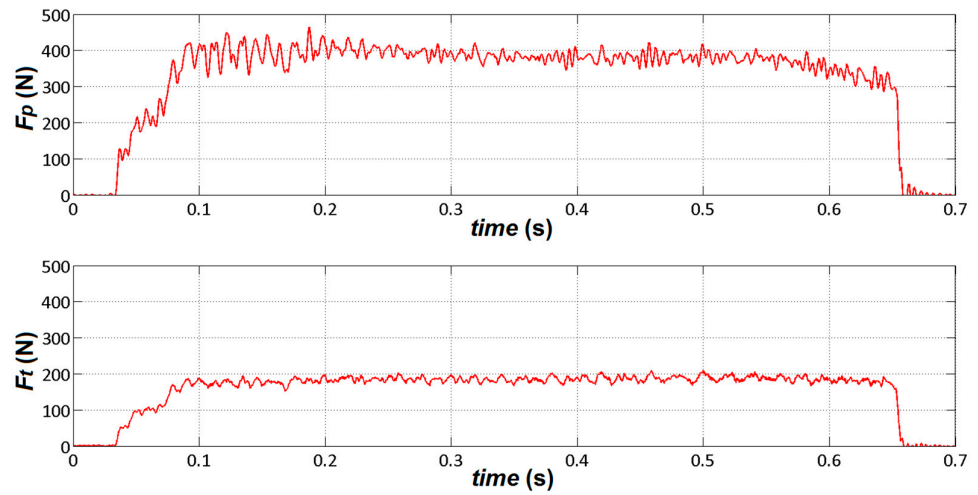


Figure 5. F_p and F_t versus time for rectangular specimens with polycarbonate ($\theta = 45^\circ$, $\gamma = 0^\circ$, $\alpha = 30^\circ$, $a_c = 0.20$ mm, and $v_c = 25$ m/min).

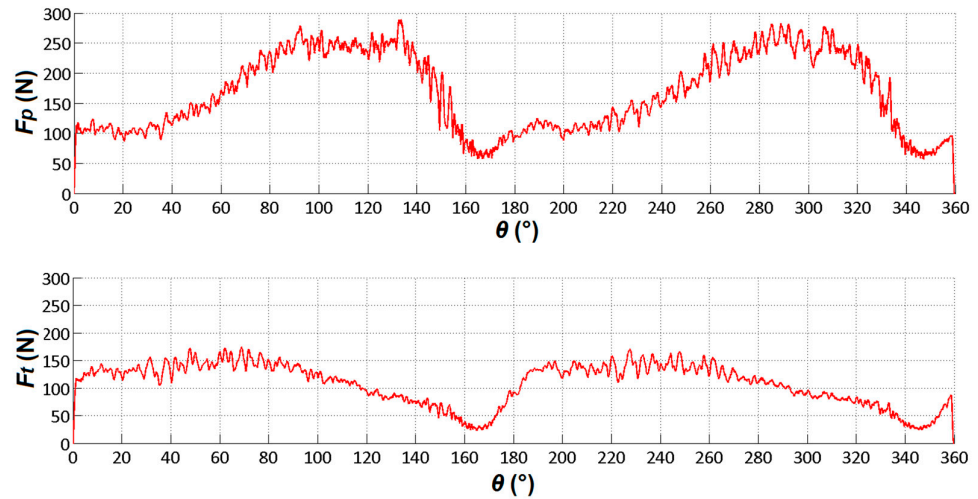


Figure 6. F_p and F_t versus θ for circular specimens without polycarbonate ($\gamma = 0^\circ$, $\alpha = 30^\circ$, $a_c = 0.10$ mm, and $v_c = 25$ m/min).

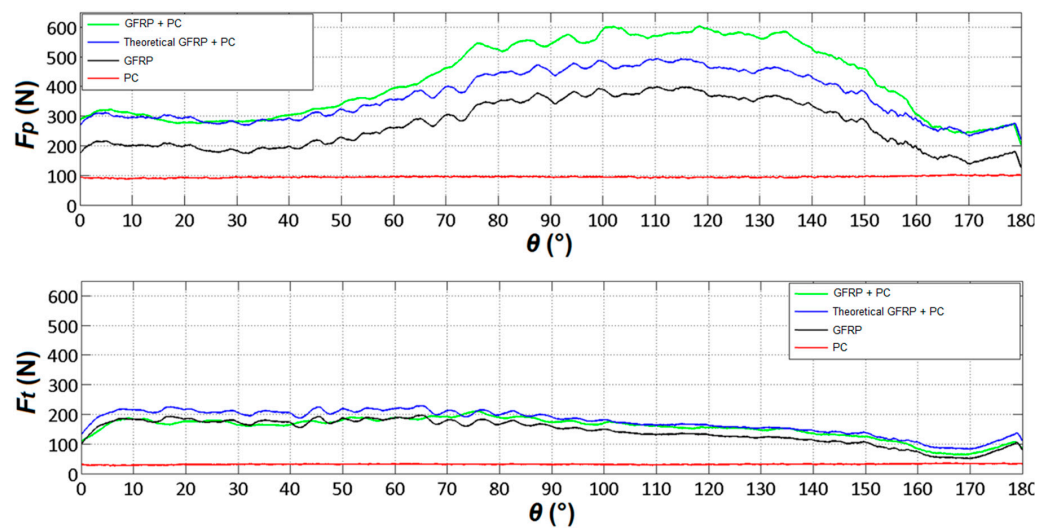


Figure 7. F_p and F_t versus θ for circular specimens with and without polycarbonate ($\gamma = 0^\circ$, $\alpha = 30^\circ$, $a_c = 0.20$ mm, and $v_c = 25$ m/min).

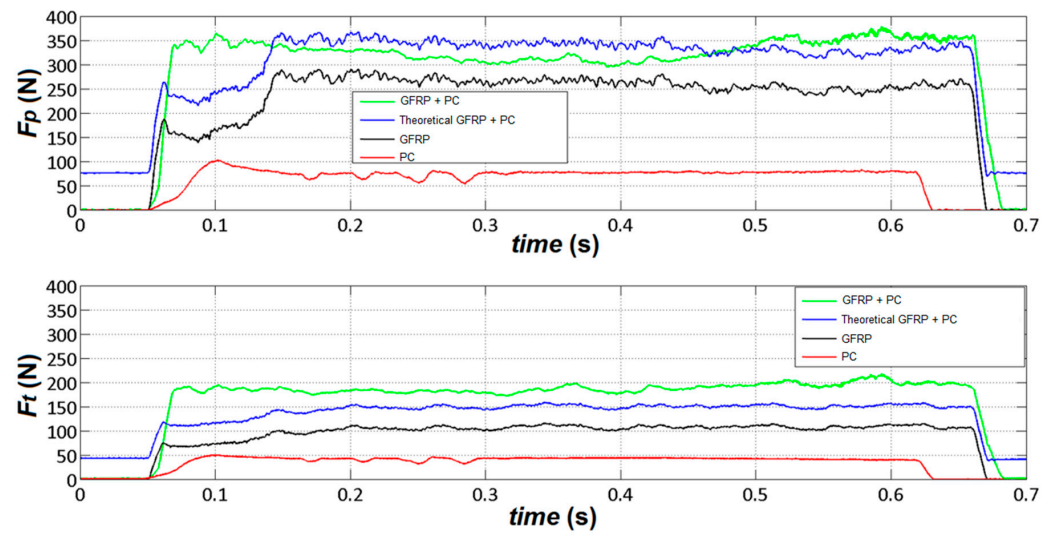


Figure 8. F_p and F_t versus time for rectangular specimens with and without polycarbonate ($\theta = 90^\circ$, $\gamma = 0^\circ$, $\alpha = 30^\circ$, $a_c = 0.20$ mm, and $v_c = 25$ m/min).

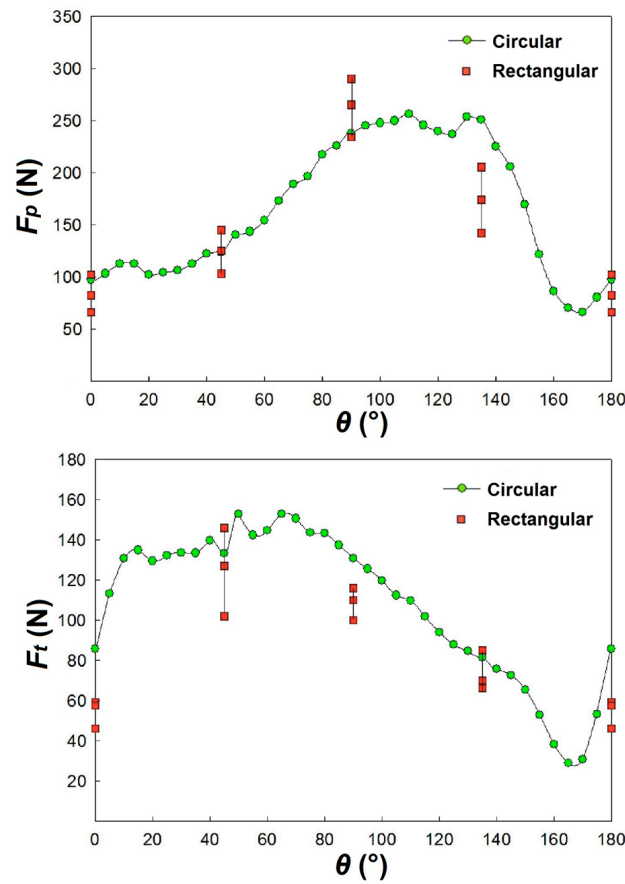


Figure 9. F_p and F_t versus θ for circular and rectangular specimens without polycarbonate ($\gamma = 0^\circ$, $\alpha = 30^\circ$, $a_c = 0.10$ mm, and $v_c = 25$ m/min).

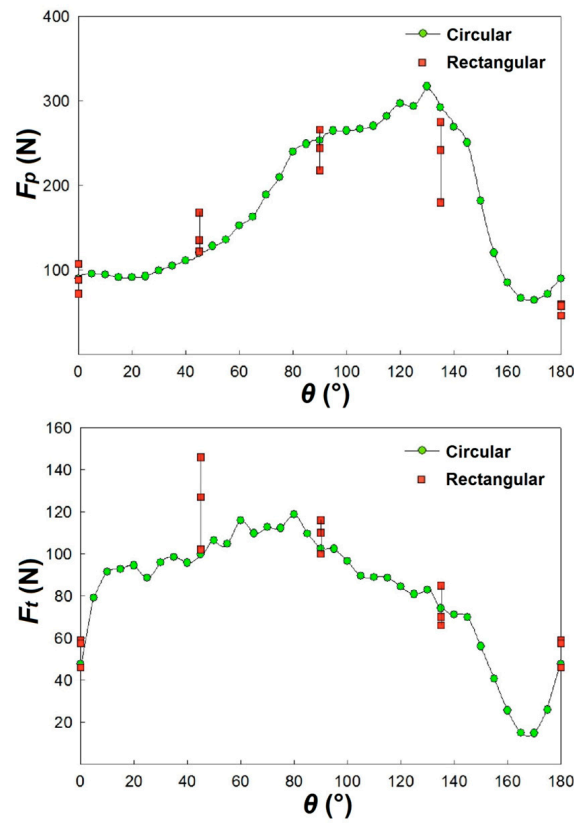


Figure 10. F_p and F_t versus θ for circular and rectangular specimens with polycarbonate ($\gamma = 0^\circ$, $\alpha = 30^\circ$, $a_c = 0.10$ mm, and $v_c = 25$ m/min).

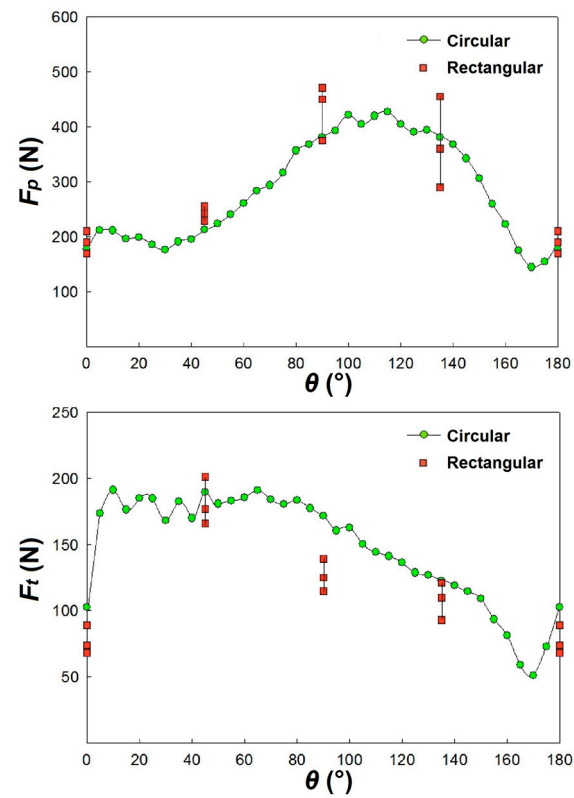


Figure 11. F_p and F_t versus θ for circular and rectangular specimens without polycarbonate ($\gamma = 0^\circ$, $\alpha = 30^\circ$, $a_c = 0.20$ mm, and $v_c = 25$ m/min).

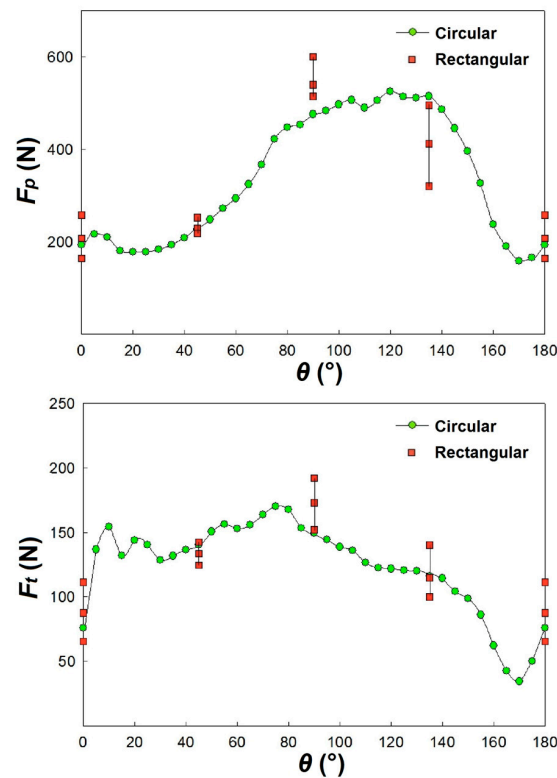


Figure 12. F_p and F_t versus θ for circular and rectangular specimens with polycarbonate ($\gamma = 0^\circ$, $\alpha = 30^\circ$, $a_c = 0.20$ mm, and $v_c = 25$ m/min).

For rectangular specimens, the forces assume the typical trends reported in Figure 5.

In the case of the circular specimens, F_p and F_t tend to increase within the second or third turns; then, after some turns, a steady state is achieved. For this reason, the trend in cutting forces is monitored from the stationary phase to prevent tool wear from influencing the force values, particularly F_t , which is much more sensitive to tool wear than F_p when machining composites [34,35]. From the recorded data, it is possible to obtain F_p and F_t as a function of θ (Figure 6). The values of θ cover the range of $0^\circ \div 360^\circ$, which corresponds to a complete revolution of the specimen. The trend of F_p and F_t is periodic, with a period of 180° ; therefore, the same cutting conditions occur when, during each revolution of the specimen, θ assumes the values of 0° , 180° , and 360° .

From the figure, it is possible to observe that the cutting forces are very sensitive to θ , reflecting the high anisotropy of UD composites. The oscillations of F_p and F_t are due to the formation of a discontinuous chip during the cutting of these materials.

To consider the influence of burrs, Figures 6 and 7 depict the typical trend of cutting forces for the circular and rectangular ($\theta = 90^\circ$) specimens, respectively, with a fixed depth of cut of 0.2 mm. In these figures, four curves are presented with the following labels:

- The “GFRP” curve represents specimens made solely of GFRP.
- The “GFRP + PC” curve represents specimens made of GFRP with additional external layers of polycarbonate.
- The “PC” curve represents specimens made only with two layers of polycarbonate.
- The “Theoretical GFRP + PC” curve is derived by summing the values of the “GFRP” and “PC” curves.

The effect of the burrs is evident for F_p . Indeed, the “theoretical GFRP + PC” curve is lower than the “GFRP + PC” one. For F_t , these effects are not so evident. Overall, the difference between these values is the additional force that is necessary to avoid the formation of burrs and to cut the material completely. The rectangular specimens cannot

highlight these differences, because of the difficulty in reaching regime conditions of the data for such very short tests.

Figures 9–12 summarize F_p and F_t for the circular and rectangular specimens in the range of $0^\circ \div 180^\circ$ for θ .

The trends of F_p and F_t related to the tests carried out on GFRP specimens with additional external layers of polycarbonate are adjusted by subtracting the contribution of polycarbonate as built. Indeed, by comparing the trends of “GFRP + PC” and “Theoretical GFRP + PC”, it is possible to understand the effective extra cutting force arising from the presence of the burr. For the circular specimens, a typical curve obtained by applying the moving average and representative of all recorded data is reported (since for circular specimens, it is possible to obtain results for all θ angles). On the other hand, for the rectangular specimens (where acquisitions are not available for all θ values), the maximum, mean, and minimum value recorded for the steady state of the curve for each specific value of θ is plotted.

In the case of the circular specimens, the cut time can be higher than 10–15 s without the variation in cutting conditions, especially when circular specimens with a greater diameter are used. In the case of the rectangular specimens, the contact time of the tool with the specimen is very short due to its small length, especially when v_c is very high. In fact, the cutting time for the tests at $v_c = 25$ m/min is only about 0.6 s. This causes greater difficulty in recording the cutting forces compared to the case of the circular specimens.

Greater differences are noted for $\theta = 45^\circ$ and 135° , while minor ones are observed for $\theta = 0^\circ$ and 90° .

Finally, it is possible to note that F_p and F_t assume the same trend in the two types of specimens.

3.3. Surface Roughness

Surface roughness measurements are performed on each of the four specified θ values for rectangular specimens. The parameter used to measure surface roughness is S_a (arithmetical mean height). It quantifies the arithmetic mean of the absolute deviations of surface profile heights from the mean line. For the circular specimens, measurements were conducted every 15° within the range from 0° to 180° . On each specimen, three surfaces were acquired, and the surface roughness results were then averaged.

Figure 13 shows the average values of S_a for the circular and rectangular specimens with polycarbonate, for both depths of cut, i.e., $a_c = 0.20$ mm and $a_c = 0.10$ mm ($\gamma = 0^\circ$, $\alpha = 30^\circ$, and $v_c = 25$ m/min). Continuous measurement with circular specimens allows for a proper trend of S_a as a function of θ to be obtained.

Looking at Figure 13, it is possible to note that for the circular specimens, the trend of S_a is similar to that of F_p (Figure 12), meaning that θ is the parameter that most influences the surface roughness. Also, considering the rectangular specimens, the results obtained at specific θ values are comparable with those obtained for the circular specimens. The results were summarized in Tables 3 and 4.

Table 3. Average and standard deviations of S_a versus θ for circular and rectangular specimens with polycarbonate ($\gamma = 0^\circ$, $\alpha = 30^\circ$, $a_c = 0.20$ mm, and $v_c = 25$ m/min).

θ ($^\circ$)	Circular Specimens		Rectangular Specimens	
	Average (μm)	St. Dev. (μm)	Average (μm)	St. Dev. (μm)
0	2.51	0.16	2.83	0.24
15	2.21	0.33		
30	2.69	0.29		
45	3.62	0.47	3.57	0.18
60	3.33	0.28		
75	4.21	0.59		
90	5.07	0.52		
105	6.35	0.34		

Table 3. Cont.

θ ($^\circ$)	Circular Specimens		Rectangular Specimens	
	Average (μm)	St. Dev. (μm)	Average (μm)	St. Dev. (μm)
120	9.09	0.02	15.63	4.26
135	12.31	2.63		
150	17.98	2.33		
165	9.46	2.10	2.83	0.24
180	2.51	0.16		

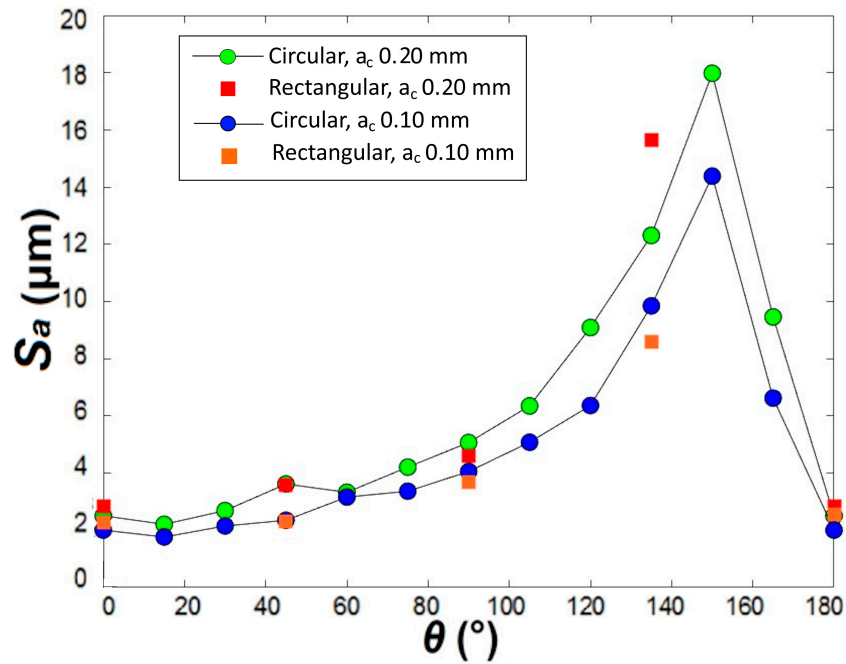


Figure 13. S_a versus θ for circular and rectangular specimens with polycarbonate ($\gamma = 0^\circ$, $\alpha = 30^\circ$, $a_c = 0.20$ mm, and $v_c = 25$ m/min).

Table 4. Average and standard deviations of S_a versus θ for circular and rectangular specimens with polycarbonate ($\gamma = 0^\circ$, $\alpha = 30^\circ$, $a_c = 0.10$ mm, and $v_c = 25$ m/min).

θ ($^\circ$)	Circular Specimens		Rectangular Specimens	
	Average (μm)	St. Dev. (μm)	Average (μm)	St. Dev. (μm)
0	2.01	0.11	2.264	0.51
15	1.768	0.24	2.3205	0.69
30	2.152	0.19		
45	2.353	0.21		
60	3.1635	0.12	3.688	0.37
75	3.368	0.39		
90	4.056	0.14		
105	5.08	0.34	8.5965	2.42
120	6.363	0.02		
135	9.848	0.69		
150	14.384	2.01	2.547	0.89
165	6.622	0.15		
180	2.008	0.32		

The lowest value is measured for $\theta = 0^\circ$, while the highest is observed for $\theta = 150^\circ$. High variability in the data, attributed to the degradation of the machined surface, is also recorded in the range from 135° to 165° .

3.4. Chip and Cutting Surface Morphology

Before presenting the results related to chip morphology and the quality of the cutting surfaces and in order to better understand the above-mentioned features, some observations on the cutting forces for the second set of tests are highlighted below.

Given the large number of process parameter combinations, Figures 14–16 are representative of three specific cutting conditions.

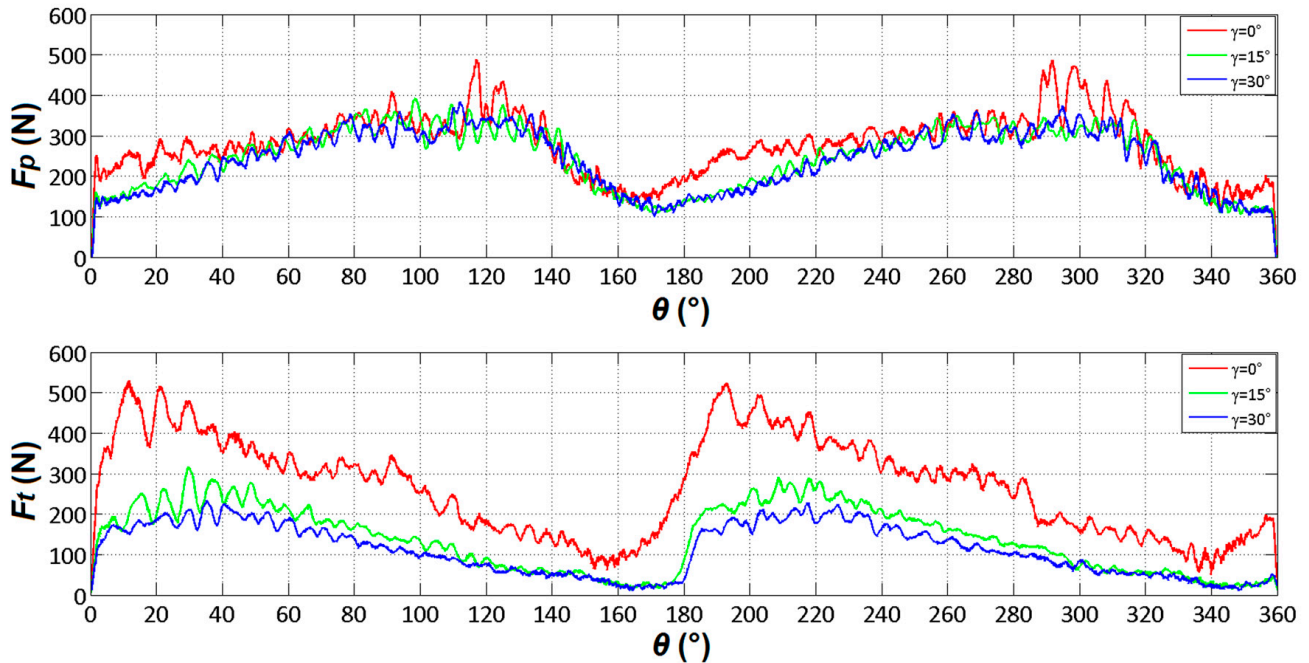


Figure 14. F_p and F_t versus θ for different γ values ($\alpha = 15^\circ$, $a_c = 0.20$ mm, and $v_c = 50$ m/min).

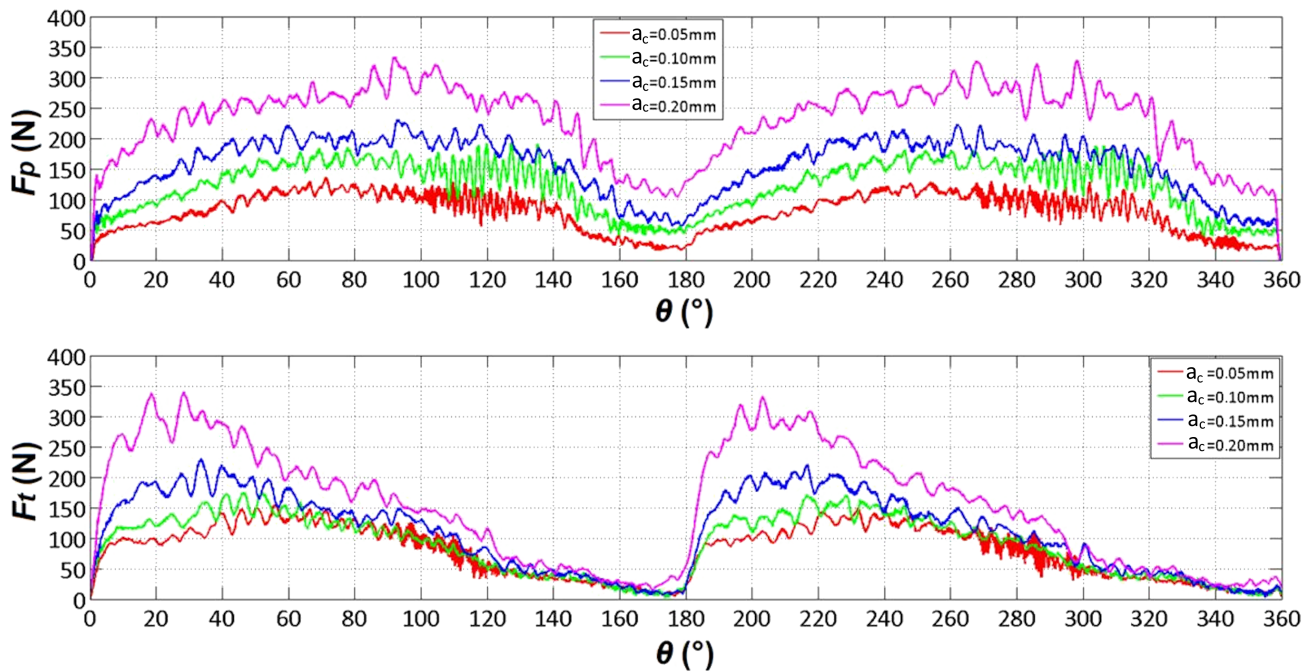


Figure 15. F_p and F_t versus θ for different t values ($\gamma = 30^\circ$, $\alpha = 15^\circ$, and $v_c = 50$ m/min).

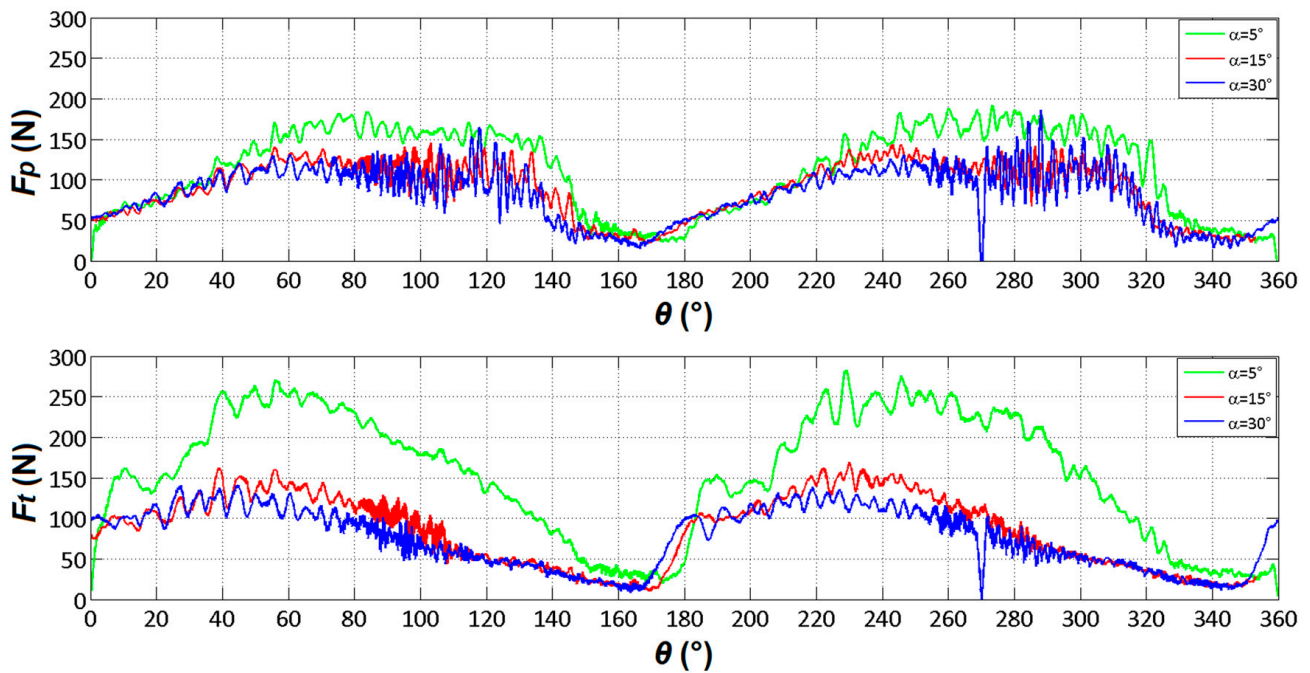


Figure 16. F_p and F_t versus θ for different α values ($\gamma = 15^\circ$, $a_c = 0.05$ mm, and $v_c = 50$ m/min).

Figure 14 shows the trend of F_p and F_t for $\gamma = 0^\circ, 15^\circ$, and 30° , $\alpha = 15^\circ$, and $a_c = 0.20$ mm. Therefore, the effect of γ on the cutting forces is evaluated for the maximum depth of cut a_t and a median value of α ($\alpha = 15^\circ$). F_p seems to remain unaffected by variations in the angle γ , while F_t displays distinct behavioral differences between $\gamma = 0^\circ$ and $\gamma > 0^\circ$. Specifically, F_t decreases as γ increases. The minimum F_t trend is obtained for $\gamma = 30^\circ$.

For this reason, the following analysis was conducted by fixing $\gamma = 30^\circ$. Figure 15 depicts the trend of F_p and F_t for $a_c = 0.05$ mm, 0.10 mm, 0.15 mm, and 0.20 mm, with $\gamma = 30^\circ$ and $\alpha = 15^\circ$. Both components of the cutting force exhibit an increase with the depth of cut, a_c . The minimum trend for both force components, F_t and F_p , is obtained for $a_c = 0.05$ mm.

For this reason, the following analysis was conducted by fixing the depth of cut, $a_c = 0.05$ mm. Figure 16 illustrates the behavior of F_p and F_t for $\alpha = 5^\circ, 15^\circ$, and 30° , with $\gamma = 15^\circ$ and a depth of cut of 0.05 mm. Notably, there is a significant decrease in the forces observed when transitioning from $\alpha = 5^\circ$ to 15° . Additionally, smaller decreases are evident when progressing from $\alpha = 15^\circ$ to 30° .

3.4.1. Chip Morphology for $\theta = 0^\circ/180^\circ/360^\circ$

For the sake of brevity, images related to all angles are not included, but it was found that the greatest chip lengths were identified when the angle θ was between 160° and 180° . As an example, Figures 17 and 18 depict the chip morphology around $\theta = 180^\circ$ for $\alpha = 15^\circ$, $a_c = 0.20$ mm and, respectively, $\gamma = 0^\circ$ and 15° , for specimens with (left) and without polycarbonate (right). On the left side of the figures, a continuous polycarbonate chip is prominently visible in the foreground. Conversely, on the right side, the cutting zone appears clearer.



Figure 17. Chip morphology of circular specimens with (left) and without polycarbonate (right), around $\theta = 180^\circ$ ($\gamma = 0^\circ$, $\alpha = 15^\circ$, $a_c = 0.20$ mm, and $v_c = 50$ m/min).

The reason is that near $\theta = 180^\circ$, the fibers have an orientation such that it is easier for the tool to generate delamination inside the specimen, resulting in easier penetration and a longer chip length. To verify this, one can observe in Figures 13 and 14 a clear decrease in force near 180° . Therefore, lower cutting forces are associated with a longer chip.

This is supported by the results of the analytical model proposed by Pwu et al. [36]. They found that the formation of the longest chip can be associated with the minimum value of the cutting forces when cutting fiber-reinforced plastics perpendicular to the fiber axis. In the present investigation, this condition occurred at $\theta \approx 165^\circ$ when $\gamma = 0^\circ$ and at higher θ values for $\gamma > 0^\circ$ (this is particularly evident looking at Figure 15 where F_t remains practically constant up to $\theta = 180^\circ$).

The described mechanism is validated by the microscopic analysis of the machined surface. Figure 19 presents images at $5\times$ (left) and $10\times$ (right) magnifications of the machined surface for $\alpha = 15^\circ$, $a_c = 0.20$ mm, and varying γ values.



Figure 18. Chip morphology of circular specimens with (left) and without polycarbonate (right), around $\theta = 180^\circ$ ($\gamma = 15^\circ$, $\alpha = 15^\circ$, $a_c = 0.20$ mm, and $v_c = 50$ m/min).

In both cases ($\gamma = 0^\circ$ and $\gamma > 0^\circ$), the morphology of the cutting surface appears to be similar. An alternation in darker and lighter areas is evident. The lighter areas correspond to the glass fibers, which exhibit higher light reflectivity, while the darker areas correspond to the matrix material. The glass fibers are distinctly visible due to their exposure by crack propagation along the direction parallel to the fibers during the formation of the “longest chip”. These observations confirm the results obtained by Wang et al. [37] on the cutting mechanism in the orthogonal machining of epoxy composites reinforced by unidirectional carbon fibers when subjected to orthogonal cutting.

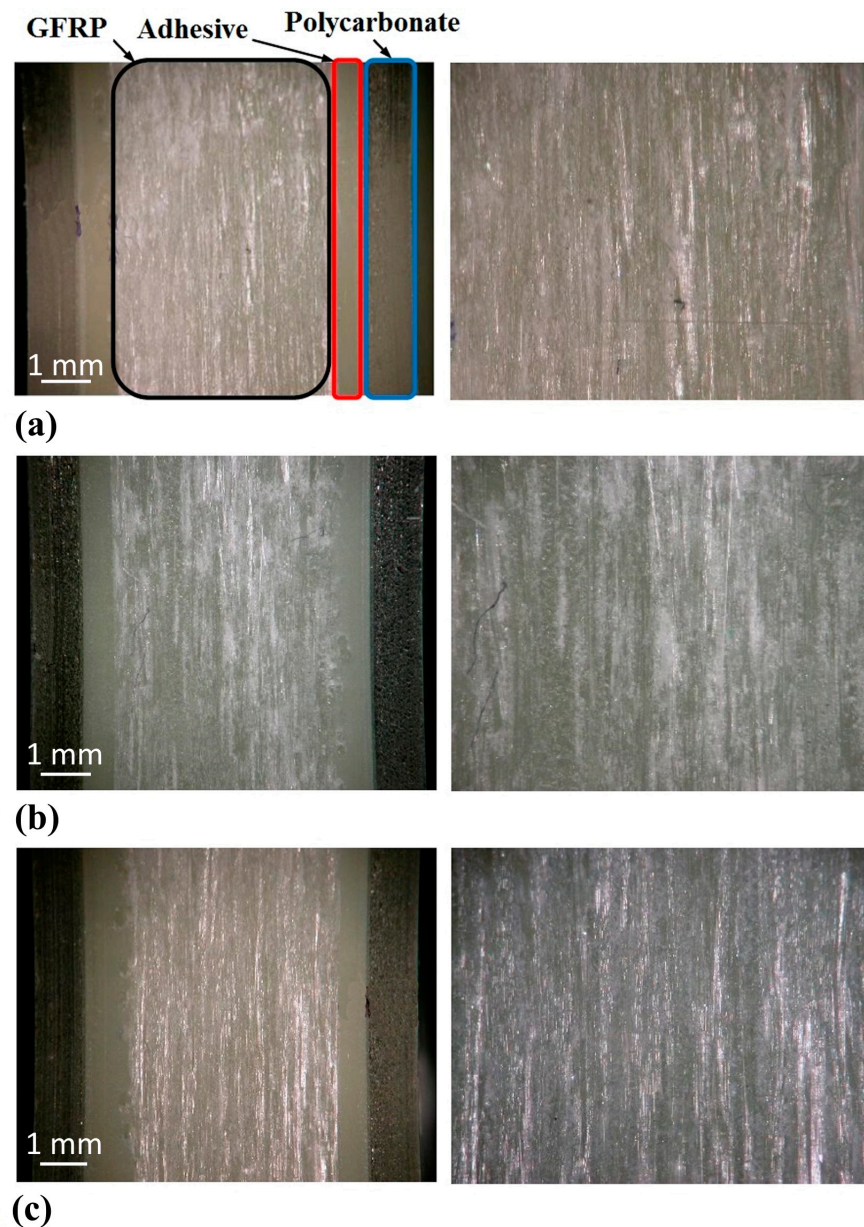


Figure 19. Characteristics of machined surface at $5\times$ (left) and $10\times$ (right) magnifications for $\theta = 180^\circ$ and (a) $\gamma = 0^\circ$, (b) $\theta = 15^\circ$, and (c) $\theta = 30^\circ$ ($\alpha = 15^\circ$, $a_c = 0.20$ mm, and $v_c = 50$ m/min).

3.4.2. Chip Morphology for $\theta = 0^\circ/180^\circ/360^\circ$

Figure 20 illustrates the chip morphology for $\gamma = 0^\circ$, $\alpha = 15^\circ$, $a_c = 0.20$ mm, and various θ values on specimens with (left) and without (right) polycarbonate. In both scenarios, a powdery chip is expelled at high velocity from the cutting area, following trajectories that align with the orientation of the fibers.

Figure 21 displays images at $5\times$ (left) and $10\times$ (right) magnifications of the machined surface for $\alpha = 15^\circ$, $\gamma = 30^\circ$, $a_c = 0.20$ mm, and various θ values.

For $\theta = 30^\circ$ (Figure 21a), the machined surface predominantly appears white due to the presence of frayed sections of the cut fibers, accompanied by slight pull-out. Scattered darker areas are observable where the fibers and the matrix have undergone a more uniform cut.

As θ increases, the surface quality deteriorates (Figure 21b,c). In these instances, some burrs can be observed on the external laminas, indicating an exacerbation of surface irregularities.

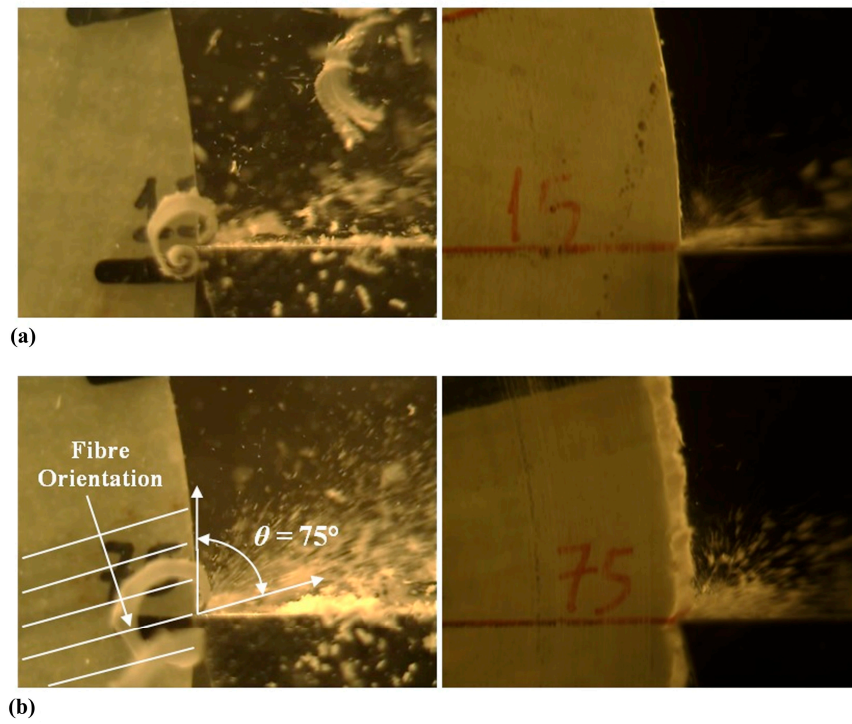


Figure 20. Chip morphology of circular specimens with (left) and without polycarbonate (right) for (a) $\theta = 15^\circ$ and (b) $\theta = 75^\circ$ ($\gamma = 0^\circ$, $\alpha = 15^\circ$, $a_c = 0.20$ mm, and $v_c = 50$ m/min).

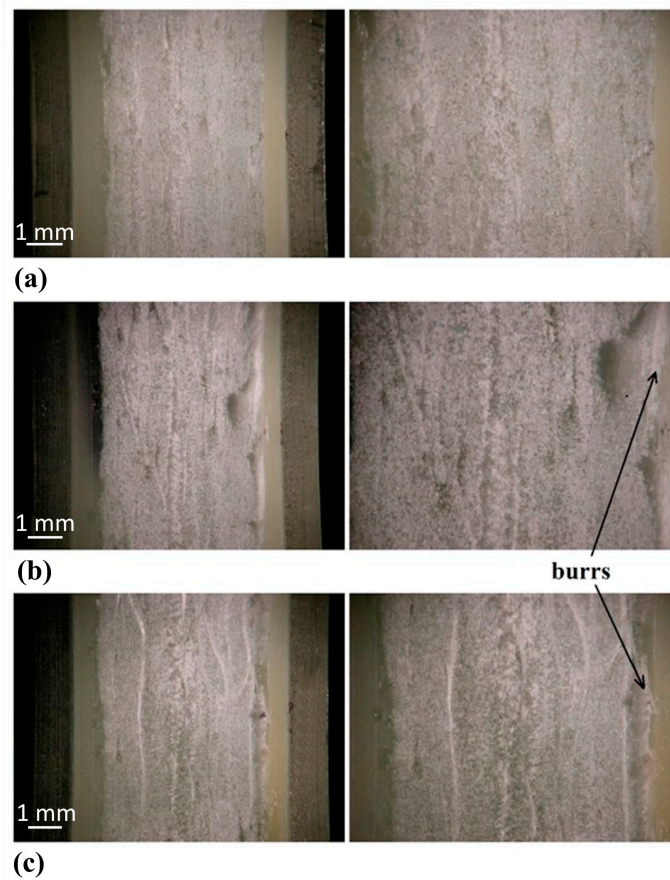


Figure 21. Characteristics of cutting surface at 5 \times (left) and 10 \times (right) magnifications for (a) $\theta = 30^\circ$, (b) $\theta = 60^\circ$, and (c) $\theta = 90^\circ$ ($\gamma = 30^\circ$, $\alpha = 15^\circ$, $a_c = 0.20$ mm, and $v_c = 50$ m/min).

Figure 22 shows images at 5× (left) and 10× (right) magnifications of the machined surface for $\theta = 90^\circ$, $\alpha = 15^\circ$, $a_c = 0.20$ mm, and varying γ values.



(a)



(b)

Figure 22. Characteristics of cutting surface at 5× (left) and 10× (right) magnifications for (a) $\gamma = 0^\circ$ and (b) $\gamma = 15^\circ$ ($\theta = 90^\circ$, $\alpha = 15^\circ$, $a_c = 0.20$ mm, and $v_c = 50$ m/min).

The surface morphology remains similar for both cases, with a slight deterioration observed for $\gamma > 0^\circ$. This observation confirms that the chip morphology within the range of $0^\circ < \theta \leq 90^\circ$ is primarily dependent on the angle θ .

3.4.3. Chip Morphology for $90^\circ < \theta < 180^\circ$

Figure 23 illustrates the chip morphology for $\gamma = 15^\circ$, $\alpha = 15^\circ$, $a_c = 0.20$ mm, and various θ values of specimens with (left) and without (right) polycarbonate.

Without polycarbonate supports, fibers can pass uncut under the tool, leading to the formation of burrs (Figure 23, right). Conversely, with polycarbonate, the outer fibers are laterally supported, enabling proper cutting (Figure 23, left).

In the range from 90° to 135° for θ , the chip appears as a powder (Figure 22a,b). Beyond 135° , the tool more easily lifts the fibers, resulting in a chip with larger dimensions (Figure 23c).

Figure 24 shows images at 5× (left) and 10× (right) magnifications of the machined surface for $\alpha = 15^\circ$, $\gamma = 15^\circ$, $a_c = 0.20$ mm, and various θ values.

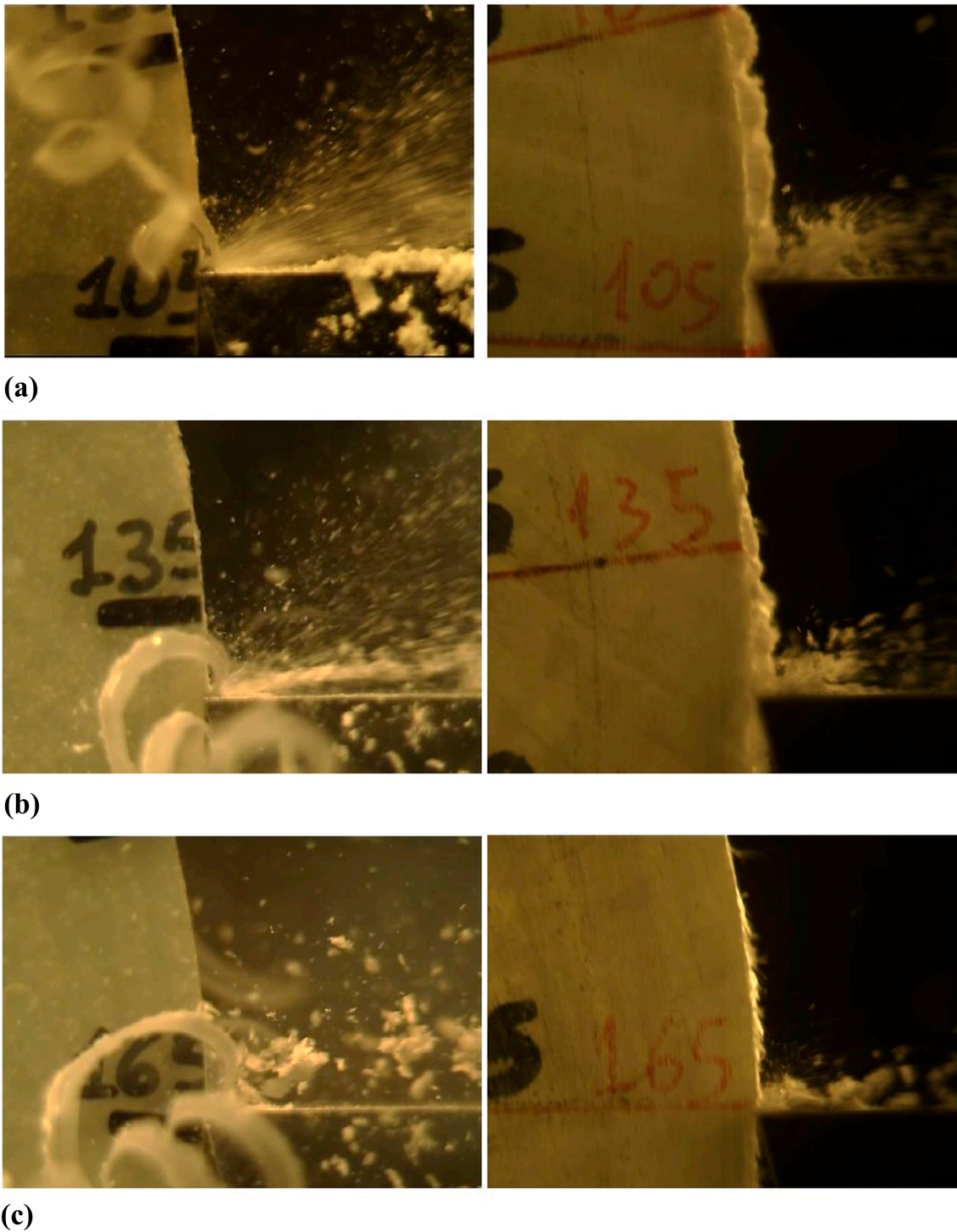


Figure 23. Chip morphology of circular specimens with (left) and without polycarbonate (right) for (a) $\theta = 105^\circ$, (b) $\theta = 135^\circ$, and (c) $\theta = 165^\circ$ ($\gamma = 15^\circ$, $\alpha = 15^\circ$, $a_c = 0.20$ mm, and $v_c = 50$ m/min).

The morphology of the machined surface takes on the appearance of a sawtooth pattern, which is particularly notable in Figure 24c.

The morphology of the machined surface is better depicted in Figure 25, where it is easy to identify darker and lighter areas (Figure 25b). The darker ones correspond to the areas where the crack propagates at the fiber–matrix interface, while the lighter ones correspond to fibers cut during tool passage (Figure 25a). These observations also confirm the findings of Wang et al. [37].

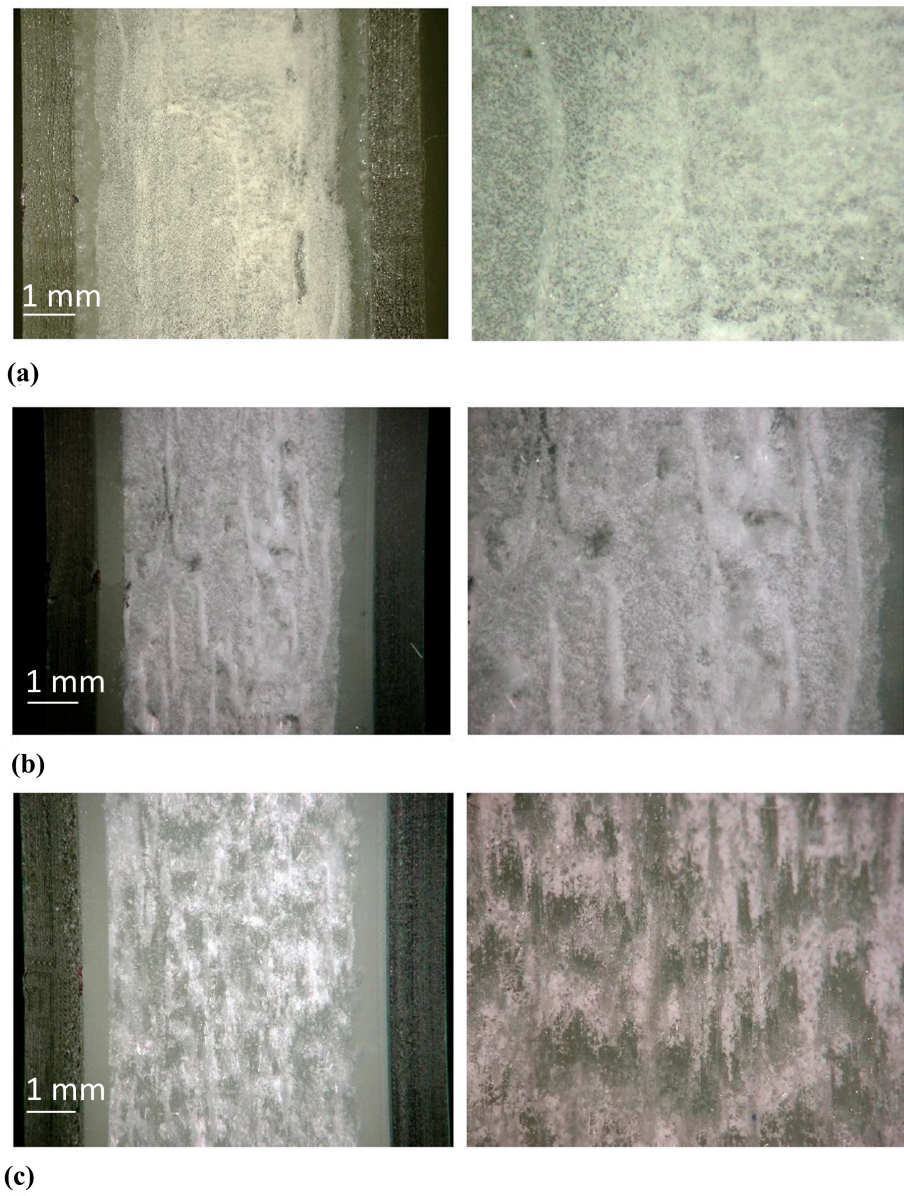


Figure 24. Characteristics of cutting surface at 5× (left) and 10× (right) magnifications for (a) $\theta = 105^\circ$, (a,b) $\theta = 135^\circ$, and (c) $\theta = 165^\circ$ ($\gamma = 15^\circ$, $\alpha = 15^\circ$, $a_c = 0.20$ mm, and $v_c = 50$ m/min).

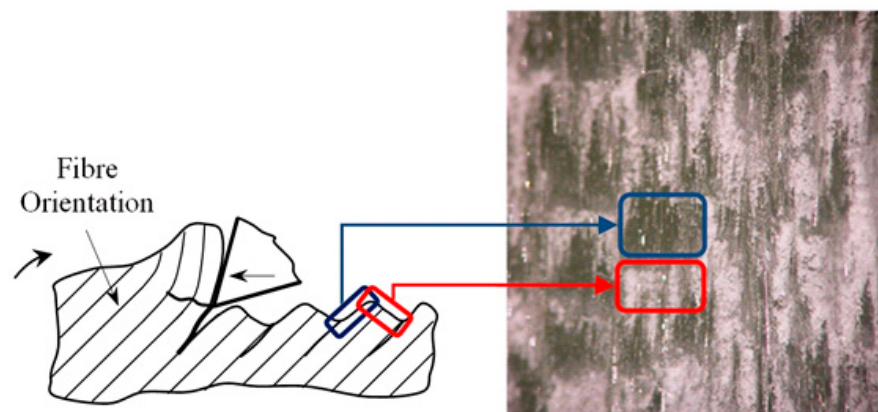


Figure 25. Details of machined surface ($\theta = 165^\circ$, $\gamma = 15^\circ$, $\alpha = 15^\circ$, $a_c = 0.20$ mm, and $v_c = 50$ m/min).

4. Conclusions

Unlike what is evident from the literature review, where in most studies, the investigation of the orthogonal cutting of composites is conducted on rectangular specimens, with consequent limitations in terms of little tool–specimen contact during cutting, low cutting speeds, and restricted values of the fiber orientation angle, in this article, we proposed and studied an experimental procedure for investigating the high-speed orthogonal cutting of UD-GFRP.

The experimental results demonstrated that circular specimens offer advantages over rectangular ones by enabling the continuous monitoring of variations in principal force and thrust force while manipulating the fiber orientation angle.

Furthermore, this study examined the influence of cutting forces on different specimen geometries and cutting conditions. It was observed that cutting forces are highly sensitive to variations in the fiber orientation angle, reflecting the anisotropic nature of UD composites. Additionally, the analysis of cutting forces highlighted the importance of accounting for the presence of burrs, as they contribute to additional cutting forces required to ensure complete material removal.

Moreover, this study investigated the roughness of machined surfaces and the morphology of chips and cutting surfaces. The findings indicate a correlation between the fiber orientation angle and surface roughness, with higher variability observed in certain angle ranges. Additionally, the morphology of chips and cutting surfaces varied depending on the cutting conditions, with notable differences observed in the presence of burrs and unsupported fibers.

In conclusion, this work not only provides an experimental methodology and valuable insights for understanding the complex phenomena arising during the cutting process of composite materials but also serves as a practical tool. The comprehensive analysis of cutting forces facilitates the development of predictive analytical and numerical models of the process and the quality of the finished product, offering clear advantages in industrial contexts. Furthermore, it is important to emphasize that although this study focused on GFRP, the methodology is flexible and applicable to all types of fiber-reinforced materials.

Author Contributions: Conceptualization, A.L.; methodology, A.L. and G.V.; software, G.V. and M.P.; validation, L.B. and A.F.; formal analysis, L.B., A.F., M.P. and G.V.; investigation, G.V. and A.L.; resources, A.L.; data curation, L.B., A.F., M.P. and G.V.; writing—original draft preparation, L.B., A.F., M.P. and G.V.; writing—review and editing, M.P. and L.B.; visualization, L.B., A.F., M.P. and G.V.; supervision, L.B., A.F. and A.L.; project administration, A.L.; funding acquisition, A.L. All authors have read and agreed to the published version of the manuscript.

Funding: This research received no external funding.

Data Availability Statement: The raw data supporting the conclusions of this article will be made available by the authors on request.

Conflicts of Interest: The authors declare no conflicts of interest.

References

1. Hsissou, R.; Seghiri, R.; Benzekri, Z.; Hilali, M.; Rafik, M.; Elharfi, A. Polymer composite materials: A comprehensive review. *Compos. Struct.* **2021**, *262*, 113640. [[CrossRef](#)]
2. Sajan, S.; Philip Selvaraj, D. A review on polymer matrix composite materials and their applications. *Mater. Today Proc.* **2021**, *47*, 5493–5498. [[CrossRef](#)]
3. Ozkan, D.; Gok, M.S.; Karaoglanli, A.C. Carbon Fiber Reinforced Polymer (CFRP) Composite Materials, Their Characteristic Properties, Industrial Application Areas and Their Machinability. In *Engineering Design Applications III: Structures, Materials and Processes*; Öchsner, A., Altenbach, H., Eds.; Springer: Berlin/Heidelberg, Germany, 2020; pp. 235–253.
4. Seo, J.; Kim, D.Y.; Dong Kim, D.C.; Park, H.W. Recent Developments and Challenges on Machining of Carbon Fiber Reinforced Polymer Composite Laminates. *Int. J. Precis. Eng. Manuf.* **2021**, *22*, 2027–2044. [[CrossRef](#)]
5. He, Y.; Sheikh-Ahmad, J.; Zhu, S.; Zhao, C. Cutting Force Analysis Considering Edge Effects in the Milling of Carbon Fiber Reinforced Polymer Composite. *J. Mater. Process Technol.* **2020**, *279*, 116541. [[CrossRef](#)]

6. Storchak, M.; Stehle, T.; Möhring, H.-C. Numerical Modeling of Cutting Characteristics during Short Hole Drilling: Modeling of Kinetic Characteristics. *J. Manuf. Mater. Process.* **2023**, *7*, 195. [CrossRef]
7. Storchak, M.; Stehle, T.; Möhring, H.-C. Numerical Modeling of Titanium Alloy Ti10V2Fe3Al Milling Process. *J. Manuf. Mater. Process.* **2023**, *7*, 1. [CrossRef]
8. Panico, M.; Durante, M.; Langella, A.; Boccarusso, L. One-Shot Drilling Process for Thin CFRP/Aluminium Alloys Stacks. *Mater. Manuf. Process.* **2024**, *in press*. [CrossRef]
9. Seeholzer, L.; Kneubühler, F.; Grossenbacher, F.; Wegener, K. Tool Wear and Spring Back Analysis in Orthogonal Machining Unidirectional CFRP with Respect to Tool Geometry and Fibre Orientation. *J. Adv. Manuf. Technol.* **2021**, *115*, 2905–2928. [CrossRef]
10. El-Ghaoui, K.; Chatelain, J.-F.; Ouellet-Plamondon, C. Effect of Graphene on Machinability of Glass Fiber Reinforced Polymer (GFRP). *J. Manuf. Mater. Process.* **2019**, *3*, 78. [CrossRef]
11. Durante, M.; Boccarusso, L.; De Fazio, D.; Langella, A. Circular Cutting Strategy for Drilling of Carbon Fiber-Reinforced Plastics (CFRPs). *Mater. Manuf. Process.* **2019**, *34*, 554–566. [CrossRef]
12. Panico, M.; Durante, M.; Langella, A.; Boccarusso, L. Numerical and theoretical approach to evaluate the clamping force and the interlayer gap extent during drilling of stacked materials. *Proc. Inst. Mech. Eng. Part B* **2024**, *in press*. [CrossRef]
13. Bolat, Ç.; Karakılınç, U.; Yalçın, B.; Öz, Y.; Yavaş, Ç.; Ergene, B.; Ercetin, A.; Akkoyun, F. Effect of Drilling Parameters and Tool Geometry on the Thrust Force and Surface Roughness of Aerospace Grade Laminate Composites. *Micromachines* **2023**, *14*, 1427. [CrossRef] [PubMed]
14. Maegawa, S.; Morikawa, Y.; Hayakawa, S.; Itoigawa, F.; Nakamura, T. Mechanism for Changes in Cutting Forces for Down-Milling of Unidirectional Carbon Fiber Reinforced Polymer Laminates: Modeling and Experimentation. *Int. J. Mach. Tools Manuf.* **2016**, *100*, 7–13. [CrossRef]
15. Geier, N. Influence of fibre orientation on cutting force in up down milling of UD-CFRP composites. *Int. J. Adv. Manuf. Technol.* **2020**, *111*, 881–893. [CrossRef]
16. Meng, Q.; Cai, J.; Cheng, H.; Zhang, K. Investigation of CFRP cutting mechanism variation and the induced effects on cutting response and damage distribution. *Int. J. Adv. Manuf. Technol.* **2020**, *106*, 2893–2907. [CrossRef]
17. Li, H.; Qin, X.; He, G.; Jin, Y.; Sun, D.; Price, M. Investigation of Chip Formation and Fracture Toughness in Orthogonal Cutting of UD-CFRP. *J. Adv. Manuf. Technol.* **2016**, *82*, 1079–1088. [CrossRef]
18. Chen, L.; Zhang, K.; Cheng, H.; Qi, Z.; Meng, Q. A Cutting Force Predicting Model in Orthogonal Machining of Unidirectional CFRP for Entire Range of Fiber Orientation. *J. Adv. Manuf. Technol.* **2017**, *89*, 833–846. [CrossRef]
19. Wang, B.; Liu, Z.; Cai, Y.; Luo, X.; Ma, H.; Song, Q.; Xiong, Z. Advancements in Material Removal Mechanism and Surface Integrity of High Speed Metal Cutting: A Review. *Int. J. Mach. Tools Manuf.* **2021**, *166*, 103744. [CrossRef]
20. Slamani, M.; Chatelain, J.-F. A Review on the Machining of Polymer Composites Reinforced with Carbon (CFRP), Glass (GFRP), and Natural Fibers (NFRP). *Discov. Mech. Eng.* **2023**, *2*, 4. [CrossRef]
21. Slamani, M.; Chatelain, J.F.; Hamedanianpour, H. Comparison of two models for predicting tool wear and cutting force components during high speed trimming of CFRP. *Int. J. Mater. Form.* **2015**, *8*, 305–316. [CrossRef]
22. Uhlmann, E.; Richarz, S.; Sammler, F.; Hufschmied, F. High Speed Cutting of Carbon Fibre Reinforced Plastics. *Procedia Manuf.* **2016**, *6*, 113–123. [CrossRef]
23. Pecat, O.; Rentsch, R.; Brinksmeier, E. Influence of Milling Process Parameters on the Surface Integrity of CFRP. *Procedia CIRP* **2012**, *1*, 466–470. [CrossRef]
24. An, Q.; Cai, C.; Cai, X.; Chen, M. Experimental Investigation on the Cutting Mechanism and Surface Generation in Orthogonal Cutting of UD-CFRP Laminates. *Compos. Struct.* **2019**, *230*, 111441. [CrossRef]
25. Voss, R.; Seeholzer, L.; Kuster, F.; Wegener, K. Analytical Force Model for Orthogonal Machining of Unidirectional Carbon Fibre Reinforced Polymers (CFRP) as a Function of the Fibre Orientation. *J. Mater. Process. Technol.* **2019**, *263*, 440–469. [CrossRef]
26. Zhang, L.C.; Zhang, H.J.; Wang, X.M. A force prediction model for cutting unidirectional fibre-reinforced plastics. *Mach. Sci. Technol.* **2001**, *5*, 293–305. [CrossRef]
27. Calzada, K.A.; Kapoor, S.G.; DeVor, R.E.; Samuel, J.; Srivastava, A.K. Modeling and Interpretation of Fiber Orientation-Based Failure Mechanisms in Machining of Carbon Fiber-Reinforced Polymer Composites. *J. Manuf. Process* **2012**, *14*, 141–149. [CrossRef]
28. Xu, X.; Jin, X. 3-D Finite Element Modeling of Sequential Oblique Cutting of Unidirectional Carbon Fiber Reinforced Polymer. *Compos. Struct.* **2021**, *256*, 113127. [CrossRef]
29. Mates Italiana. Available online: https://fileserv.mates.it/Prodotti/2_Matrici/TDS/Resine/Mates/SX10_DS.pdf (accessed on 6 April 2024).
30. Dalla Betta Group. Available online: <https://www.dallabetta.com/vetro.html> (accessed on 10 November 2023).
31. Jagadeesh, P.; Sanjay Mavinkere Rangappa, S.M.; Suyambulingam, I.; Siengchin, S.; Puttegowda, M.; Binoj, J.S.; Gorbatyuk, S.; Khan, A.; Doddamani, M.; Fiore, V.; et al. Drilling characteristics and properties analysis of fiber reinforced polymer composites: A comprehensive review. *Heliyon* **2023**, *9*, e14428. [CrossRef]
32. Wang, F.; Yin, J.; Ma, J.; Jia, Z.; Yang, F.; Niu, B. Effects of Cutting Edge Radius and Fiber Cutting Angle on the Cutting-Induced Surface Damage in Machining of Unidirectional CFRP Composite Laminates. *J. Adv. Manuf. Technol.* **2017**, *91*, 3107–3120. [CrossRef]

33. Caprino, G.; Langella, A. Analysing Cutting Forces in Machining Processes for Polymer-Based Composites. In *Machining Technology for Composite Materials*; Hocheng, H., Ed.; Elsevier: Amsterdam, The Netherlands, 2012; pp. 75–115.
34. Rathod, K.B.; Lalwani, D.I. Force Modelling in Orthogonal Cutting Considering Flank Wear Effect. *J. Inst. Eng. Ser. C* **2018**, *99*, 673–679. [[CrossRef](#)]
35. Henerichs, M.; Voß, R.; Kuster, F.; Wegener, K. Machining of Carbon Fiber Reinforced Plastics: Influence of Tool Geometry and Fiber Orientation on the Machining Forces. *CIRP J. Manuf. Sci. Technol.* **2015**, *9*, 136–145. [[CrossRef](#)]
36. Pwu, H.; Hocheng, H. Chip Formation Model of Cutting Fiber-Reinforced Plastics Perpendicular to Fiber Axis. *ASME J. Manuf. Sci. Eng.* **1998**, *120*, 192–196. [[CrossRef](#)]
37. Wang, X.M.; Zhang, L.C. An Experimental Investigation into the Orthogonal Cutting of Unidirectional Fibre Reinforced Plastics. *Int. J. Mach. Tools Manuf.* **2003**, *43*, 1015–1022. [[CrossRef](#)]

Disclaimer/Publisher’s Note: The statements, opinions and data contained in all publications are solely those of the individual author(s) and contributor(s) and not of MDPI and/or the editor(s). MDPI and/or the editor(s) disclaim responsibility for any injury to people or property resulting from any ideas, methods, instructions or products referred to in the content.